Journal of Manufacturing Processes 78 (2022) 71–81

Contents lists available at ScienceDirect

Journal of Manufacturing Processes

journal homepage: www.elsevier.com/locate/manpro

Split anode calorimetry for plasma arc energy density measurement with laser calibration

Guangyu Chen [a,*], Stewart Williams [a], Jialuo Ding [a], Yipeng Wang [b], Wojciech Suder [a]

[a] Welding Engineering and Laser Processing Centre, Cranfield University, Cranfield MK43 0AL, UK
[b] Institute of Light Alloy and Processing, Faculty of Materials and Manufacturing, Beijing University of Technology, Beijing 100124, China

ARTICLE INFO

Keywords:
Arc profile
Split anode calorimetry
Plasma arc
Welding

ABSTRACT

A split anode calorimeter (SAC) has been developed for the measurement of plasma transferred arc (PTA) energy density. A novel aspect is the use of a laser beam with a well-defined energy profile which was first measured using a commercial laser beam diagnosis system and was used to calibrate the SAC. The SAC temperature data generated profile showed the same profile measured by the laser diagnosis system. This confirmed the accuracy of the SAC method and its suitability for measuring the energy distribution of an electric arc if provided stably. The PTA energy profile was observed to be distorting when crossing over the split anode interface of the SAC. This was corrected by moving the ground wire from the side to the centre of the anode. Detailed analysis of 130A PTA energy density profiles generated from both the current density and the temperature distribution of the arc showed that the current data generated profile is narrower than that of the temperature data generated profile. This indicates that the effective energy distribution is wider than that of the width of the arc column due to other energy transfer processes such as convection and radiation. The energy absorption distribution matched well to a Gaussian distribution model with a radius of 7 mm. The arc energy absorption rate of the copper plate was measured and found to be about 56%.

1. Introduction

An electrical arc is a discharge between two electrodes, with current conducted from an electrode to a workpiece through a heated and ionised gas, the plasma. The voltage and the current in the arc determine the amount of power released, the heat from which melts the electrode and the joint faces when using an electric arc for welding [1]. The energy density profile of an electric arc typically has an axial symmetric bell-shaped distribution. This profile needs to be quantified for many reasons, for example, in the simulation of a welding process. The measured energy profile will allow more accurate modelling compared to reverse engineering. In addition, process control and understanding could also be improved if the arc energy density profile was determined as a function of different system designs and process parameters, with the best energy profiles selected for specific applications. Many researchers have studied the energy distribution of an electric arc with various kinds of methodologies being developed. Some non-invasive spectroscopic measuring methods were introduced due to the hostile condition inside an arc plasma body [2–5]. These spectroscopic methods are based on an essential assumption of local thermodynamic equilibrium (LTE) [2]. LTE requires that within a given (small) volume, element electron, ion and neutral temperatures are (approximately) equal, and thermodynamic properties (such as density, heat conductivity etc.) are virtually constant [6]. However, the validity of LTE is questionable for complex arcing conditions [7–10]. Some researchers argued that LTE is not valid for all arc regions and conditions. Some invasive methodologies were also introduced to directly detect an arc from the inside of its plasma body, e.g., the Langmuir probe [11,12] and the split anode calorimetry (SAC) [6,13–17]. The Langmuir probe method uses an electrostatic probe to measure an arc plasma body directly. It is fast and relatively easy to apply and has been shown to be viable even at high pressures where the plasma temperatures considerably exceed the melting temperature of the probe. Unfortunately, interpretation of the data produced is fraught with difficulties because no simple, comprehensive underlying theory exists [12]. The SAC method was first proposed by [13] and has been widely used to measure different kinds of heat sources, including gas tungsten arc and plasma transfer arc (PTA). Two separated non-ablating copper anodes are employed under a torch, with electrical and thermal insulation in between. Two separate cooling water circuits are placed under each of the copper plates. During the measurement, the electric

* Corresponding author:
E-mail address: guangyu.chen@cranfield.ac.uk (G. Chen).

https://doi.org/10.1016/j.jmapro.2022.04.003
Received 22 January 2022; Received in revised form 2 April 2022; Accepted 2 April 2022
Available online 16 April 2022

arc is traversed across the interface between the two anodes in equal increments. The energy of the arc plasma is then 'split' into two parts at the interface. The current going through each section of the anodes, the mass flow rate and the temperature changes of both cooling water circuits are measured. In this way, the energy amounts that two plates absorbed can be calculated. Based on this, the energy distribution of the arc can be determined when the interface scans across the arc section.

A verification experiment was introduced by Schoeck [14] to test the reliability of the SAC method. In his work, he used a point anode probe method, which consisted of a water-cooled copper probe surrounded by an insulated water-cooled copper holder to measure electric arcs and compared it with the SAC results. However, this calibration method of his device is not definitive as he used a similar unverified invasive procedure. Since then, the SAC method has been widely accepted but with limited studies investigating its accuracy and reliability. In this study, a laser beam measurement was introduced to calibrate this method. Unlike an electrical arc, a laser beam is inherently positionally stable and is not affected by other ambient factors such as position changing during measurement. Another critical point is that the energy distribution of a laser beam can be measured by other fully developed and well-verified methods. There are several methods of acquiring the intensity profile of a laser beam, such as camera-based sensors, slit scanners, knife-edge scanners and pinhole scanners [18]. The rotating hollow needle laser beam diagnosis system is one of the most versatile and effective methods [19]. By comparing the profile generated by the SAC with the profile generated by the rotating hollow needle method, the SAC's capability of measuring an energy profile can be tested and verified. The diagnostic principle of the rotating hollow needle method is based on a small pinhole on the circumference of a hollow needle probing a laser beam. Part of the laser beam that passes the pinhole is reflected inside the needle and guided to the rotating centre. It is then reflected out of the needle and measured using a pyroelectric detector. With every rotation, a cutting line through the beam is measured. The completed system of a needle with pinhole, motor and sensor is moved through the beam, in such a way that the whole beam section is scanned. Although this method is limited by the damage threshold of the material [20], a rotating hollow needle is capable of analysing the energy distribution of a laser beam [21]. Calibration and qualification of the laser profiler can be made by analysing the beam propagation behind a pinhole and compared to a theoretical calculation [22].

The results obtained by the SAC are not two-dimensional but integrated one-dimensional profiles along the moving direction of an electric arc. To convert a one-dimensional profile to a two-dimensional profile using an Abel inversion, an assumption that the arc body is axial symmetrical needs to be made [13]. Therefore, arc stability is essential for the SAC measurement. In the previous SAC measuring works, axial asymmetric distortion was found when an arc travelled across the interface, with its shape altering during the measuring process [15,16]. However, the mechanism of this phenomenon was not fully revealed. Some researchers stated that oxidation that occurred on the surface of the copper plates during the calorimetry influenced the location of an arc root [15], whereas other researchers concluded that oxide might have an influence on the current distribution but not on the arc stability [16]. A magnetic field was used to restrict the arc column from wandering [13]. But in the author's opinion, a magnetic field might change the character of an arc. The influence of grounding on arc shape, however, has not yet been analysed. In this study, the shape and position variation of a PTA when crossing the interface was investigated. Different grounding arrangements were tested, and their effects on arc distortion were revealed. Based on that, a modified SAC setup was designed to reduce arc distortion. However, as the plasma body of an electric arc is not rigid [6,15,16], random distortion seems to be inevitable during the measurement. Repeated measurements still need to be applied when measuring a single arc energy source to get an averaged result.

Finally, a typical PTA with a current intensity of 130 A was measured. The measured result was compared with a widely used Gaussian distribution model. The verification of this critical empirical model that is used in most welding simulations is essential. It was shown in this study that a Gaussian profile can be used as an approximate substitution for the actual energy profile of a PTA.

2. Methodology

2.1. Initial and modified SAC setups

Two versions of the SAC setups, both initial and modified, were tested to investigate the effect of grounding on arc distortion. Fig. 1 illustrates the initial SAC setup. Two separated cooling water slots were machined into a glass fibre reinforced polyamide holder as the lower halves of two cooling channels (Fig. 1b). Two 99.95% oxygen-free copper anodes with dimensions of 95 mm × 90 mm × 10 mm were fixed onto a polyamide holder. Water slots were machined at the bottom of the copper plates as the upper halves of the two cooling channels. Two Viton O-Ring seals were placed between the copper anodes and the polyamide holder to prevent water from leaking. Two separate cooling channels were formed when placing the copper anodes on the top of the polyamide holder. A set of brass screws were mounted in the copper slots to increase turbulence and mixing of water. Without the turbulence induced by the brass screws, the cooling water under the copper plates was heated unevenly, leading to fluctuations of the thermocouples signal. A gap between those two anodes was set using a 75 μm thick heat and electrically resistant polyamide film (DuPont® KAPTON® HN' 3 mil'). Four K-Type thermocouples were attached to the inlets and the outlets to measure the temperature changes of the cooling water. Two turbine flow meters were placed within each circuit to monitor the flow rate of the cooling water. A chiller with refrigeration was used to pump and cool down the water and provide a total flow rate of 2.7 L/min for both cooling circuits. The inlets of the cooling water were placed close to the anode interface to provide a lower water temperature for the arc section. In the initial design, two ground connectors were mounted to both the copper anodes on the opposite sides and connected to an arc power supply.

Based on the initial SAC device, a modified SAC with centred grounding was designed. The setup of the centre grounded SAC device is demonstrated in Fig. 2. Two ground wires were placed at the bottom of the plates right under the position of the arc instead of being placed at the sides of the copper plates. By using this configuration, the distance difference between the ground wires and the arc section was minimised. To allow the arc current to go through the copper anode from the upper surface to the ground connectors at the bottom, the copper plate holders need to be electrically conductive. Therefore, two separated aluminium holders instead of one polyamide holder were used to support the copper plates and enclose the water circuits.

2.2. Laser calibration experiment

The laser calibration experiment was conducted using the initial SAC setup. An IPG YLR-8000 8 kW CW fibre laser was used to generate a 1.5 kW unfocused laser beam. The power of the output laser was measured using an OPHIR LASERMETER laser power meter. A Fanuc RJ3iB robot system was used to hold and move the laser processing head. The copper plates were coated with graphite spray in this laser experiment to reduce the reflection of the laser and increase energy absorption. The graphite coating can also ensure that the measurement is stable and not affected by any surface oxidation. A PRIMES FocusMonitor FM laser diagnosis was used to measure the laser beam energy profile as a reference. The FM is a commercially available hollow needle diagnosis system that complies with the requirements of the ISO 11146 standard [23]. During the FM laser measurement, a small pinhole (typical diameter: 20 μm) in the measuring tip sampled a small part of a laser beam. The sampled part of the laser beam was guided onto a detector element, which was chosen

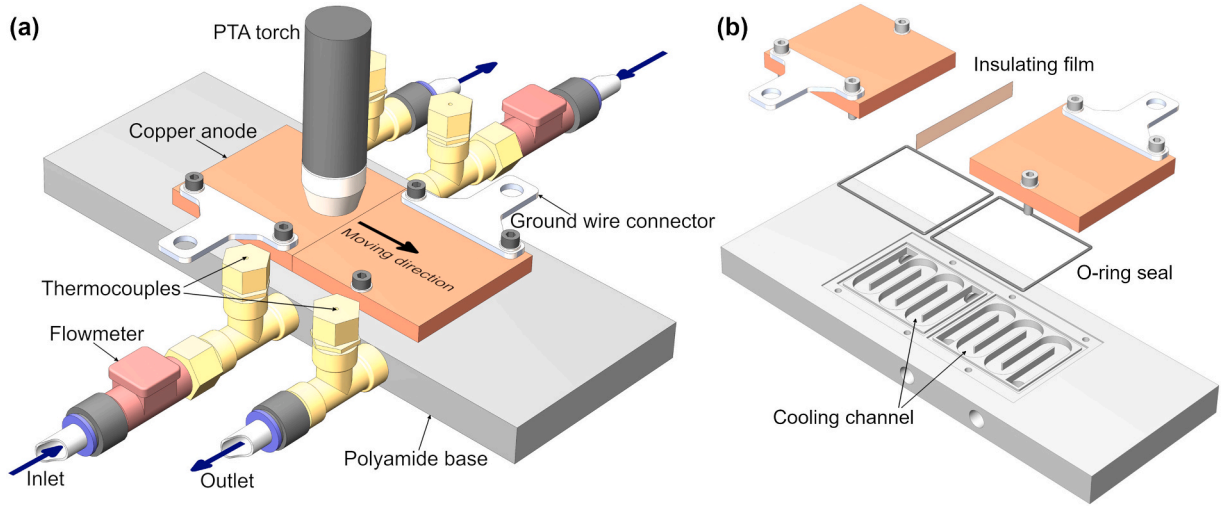

Fig. 1. (a) Setup of the initial SAC device, and (b) cooling channels machined on the polyamide base.

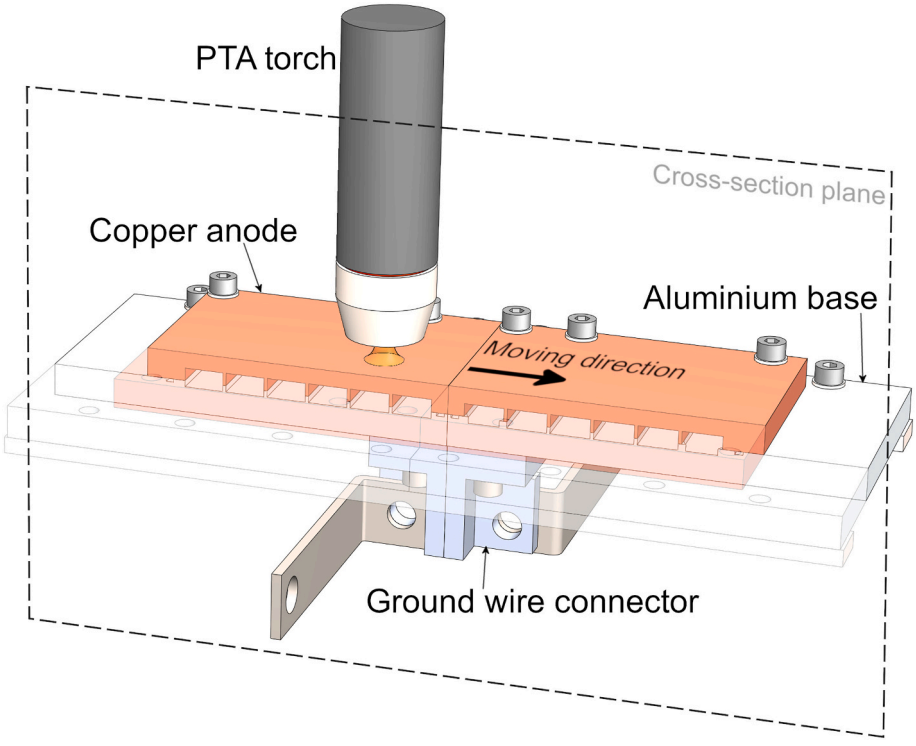

Fig. 2. The modified SAC setup with ground wires placed under the copper plates.

according to the power and the wavelength of the laser radiation. The setups of the laser measurements using both the FM and the SAC are explained in Fig. 3. For the FM measurement, the laser beam was placed vertically and was absorbed by a laser beam dump to prevent accidental damage (Fig. 3a). For the SAC measurement, the laser processing head was set to an angle of 5 degrees to the vertical to avoid reflection from the copper plate that might damage the processing head (Fig. 3b).

Parameters for the laser experiment are listed in Table 1.

2.3. PTA measurement and arc shape analysis

The whole PTA measurement setup was enclosed in a gas-tight tent filled with pure argon and purged until the oxygen level dropped below 300 ppm before the calorimetry process to avoid any possible influence of surface oxidation. The copper plate anodes were polished with 1000-grit abrasive paper to obtain very fine upper surfaces. A Fronius TransTig 5000 welding power source was used for the plasma arc calorimetry. A ZABER A-LST0250D linear actuator was used with a repeating accuracy of 63 μm to move the torch in equal increments. Parameters used for the PTA measurement are listed in Table 2.

Three different ground wire connections were arranged to study the effect of grounding position on arc shape stability, as indicated in Fig. 4. The first arrangement is the initial arrangement used in the initial SAC setup (Fig. 4a). The copper plates were insulated from each other and were both connected to ground wire connectors at the sides. In the second and third arrangements, the insulation between the anodes was removed to connect them. Two separate ground wire connectors were replaced with one ground wire connector positioned at either the right

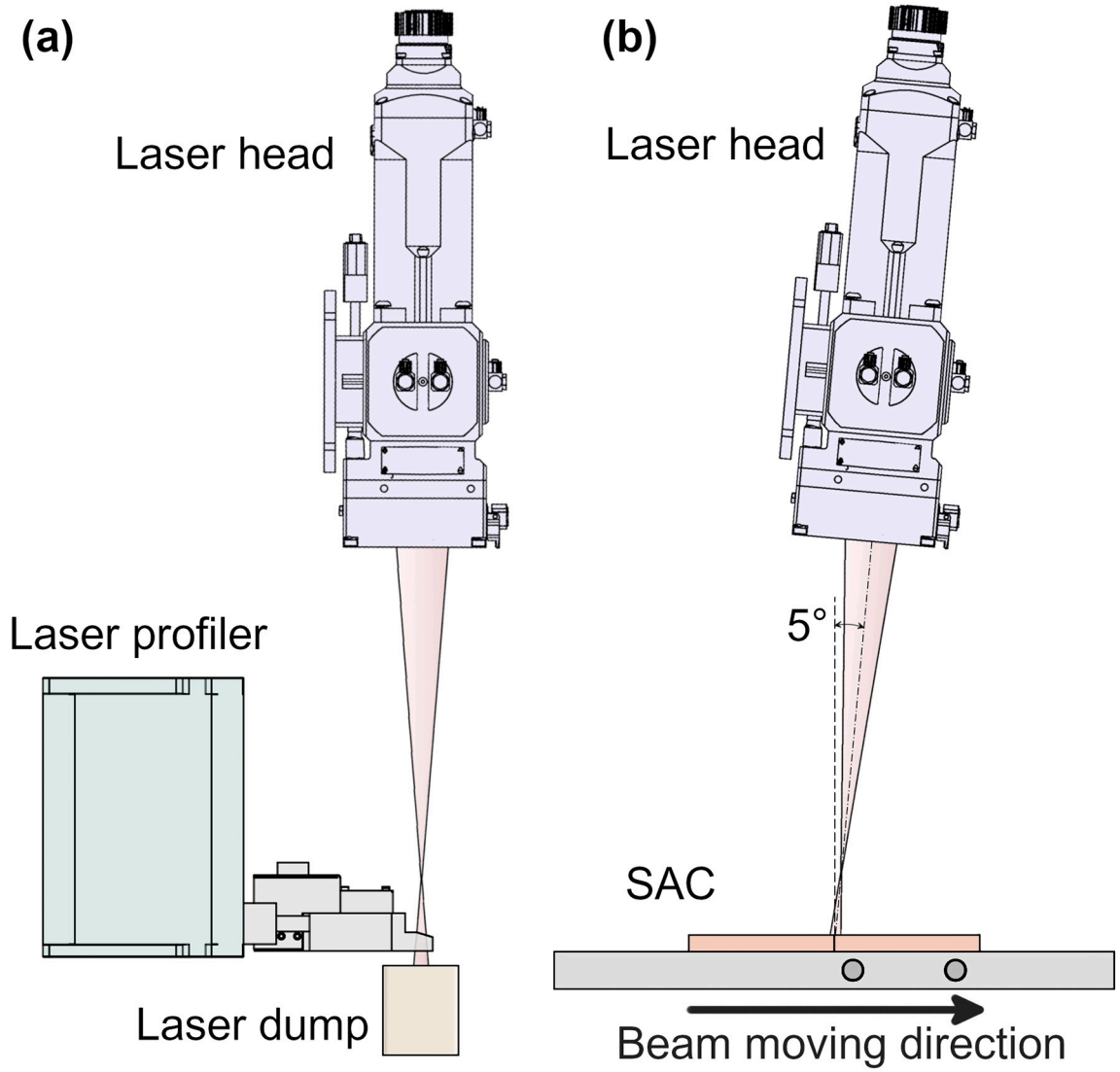

Fig. 3. Laser measurement setup: (a) with the FM, and (b) with the SAC.

Table 1
Parameters for the laser experiment.

Power/(W)	1500
Wavelength/(μm)	1.06
Focal length/(mm)	250
Distance between the laser head and the measuring plane/(mm)	305

Table 2
Parameters for the PTA experiment.

Current/(A)	130
Voltage/(V)	23.5
Plasma gas/(L/min)	0.8
Shielding gas/(L/min)	15
Distance between the torch and the anodes/(mm)	8
Orifice size/(mm)	3.9
Electrode diameter/(mm)	4
Electrode Tip Angle/(degree)	40
Electrode Tip Set-back/(mm)	2.4

or the left anode (Fig. 4b and c). A Xiris XVC-1000 camera was placed at one side of the interface to capture the shape of the arc when it crossed the interface.

2.4. Data acquiring and processing

Two National Instruments NI 9211 and NI 9361 data logger modules were used to acquire temperature and water flow rate data. A Triton P349 was used to collect current data. All experimental data were collected and recorded using Labview and processed using Excel and Origin software on a personal computer (PC). During both the experiments, the laser head and the PTA torch were moved across the interface between the copper anodes at increments of 0.2 mm. The whole interface traversing process was divided into 100 increments. A 30 s period of time was applied for each increment keeping the laser head or the welding torch stationary and allowing stabilisation of water temperature. Measurement of the water temperature was taken from the 15th second to the 30th second of each increment to ensure that a stabilised temperature was taken. The energy that each copper anode received at each increment can be calculated using either Eq. (1) with the temperature data or Eq. (2) with the current data:

$$Q_{temp} = (T_{out} - T_{in}) C_{water} M_{water} \quad (1)$$

$$Q_{current} = IU \quad (2)$$

In Eq. (1), Q_{temp} represents the energy that each anode received at each increment calculated from the temperature data, T_{out} and T_{in} are

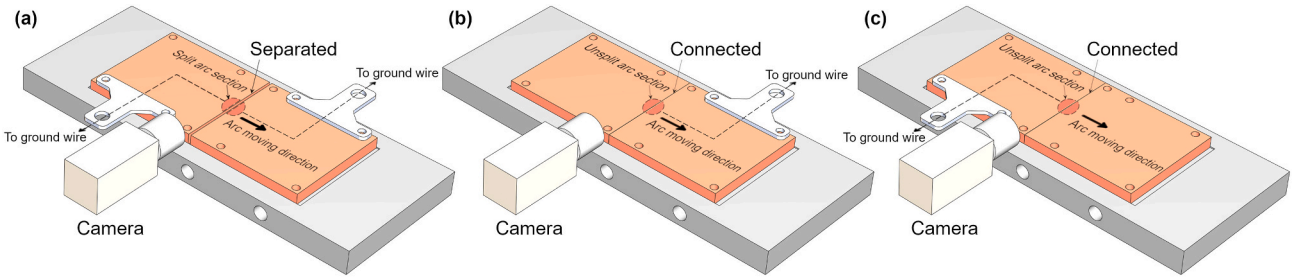

Fig. 4. Three grounding arrangements for the arc stability study: (a) grounding at both sides with an insulated interface, (b) grounding at the right side with a connected interface, and (c) grounding at the left side with a connected interface.

the water temperatures at the outlet position and the inlet position, C_{water} is the specific heat of water and M_{water} is the mass flow rate of the cooling water. In Eq. (2), $Q_{current}$ represents the energy that each anode received at each increment calculated from the current data, I is the split current that flows through each of the copper anodes, and U is the voltage of the arc. It is noteworthy that the energy amount calculated by Eqs. (1) and (2) is the partial energy received by each anode. The total energy amount should be the summation of the energy amounts received by two anodes.

The energy per increment ΔQ_i received in each 0.2 mm interval was measured using Eq. (3). Q_i represents the energy that one of the copper anodes received calculated from Eqs. (1) or (2) in each increment.

$$\Delta Q_i = Q_{i-1} - Q_i \tag{3}$$

By associating each ΔQ_i with the position of the corresponding increment, the distribution of the energy source was generated. It is worth noting that this profile is a one-dimensional profile directly converted from the acquired data. This profile represents the energy distribution along the arc advancing direction, and each point means the energy integrated along the split anode interface direction at each increment. In this study, only the directly converted one-dimensional profile will be discussed. The energy profile generated from the current data could be considered as the theoretical energy profile of the plasma body before being absorbed by the substrate, and the energy profile generated from the temperature data could be considered as the profile of the energy absorbed by the substrate surface.

Later, the resemblance between the measured profile and the Gaussian model was analysed to test the reliability of the Gaussian model. Eq. (3) is a typical Gaussian distribution formula used in welding simulation:

$$Q(x,y) = \frac{3\eta Q_{total}}{\pi r^2} exp\left[-3\left(x^2+y^2\right)/r^2\right] \tag{5}$$

where Q represents the energy density of the arc at a particular point, Q_{total} represents the total energy input of the heat source, x and y are the relative position coordinates to the centre of the heat source, r is a parameter that determines the size of the heat source, and η is the absorption rate. Since Q_{total} and η are determined in this experiment, r is the only adjustable variable to alter the Gaussian profile shape and find the best match to the measured profile. Pearson correlation coefficient

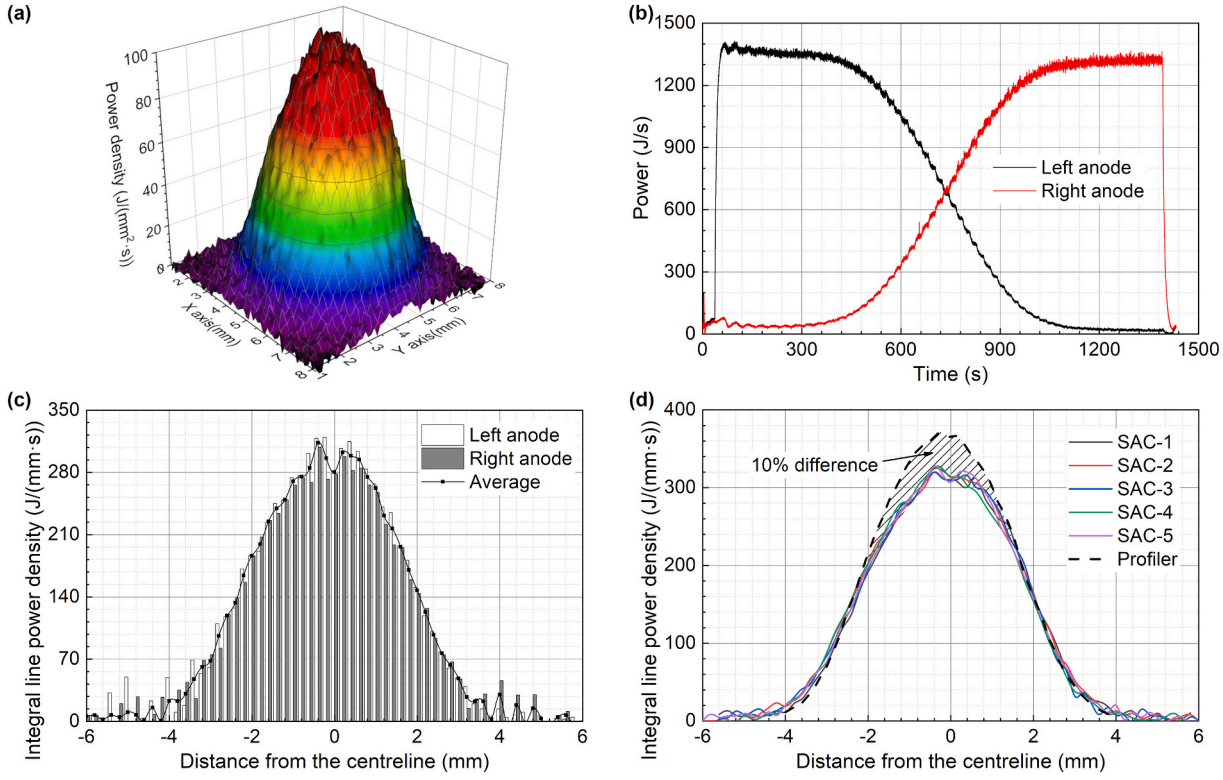

Fig. 5. Laser measurement results: (a) laser beam energy distribution on a two-dimensional plane, (b) energy that goes through two anodes calculated from the temperature data, (c) laser beam energy profile generated by the SAC, and (d) comparison of the profiles generated by the SAC and the FM.

(PCC) [24] was calculated to evaluate the correlations between the measured profiles and Gaussian models.

3. Results and discussion

3.1. SAC calibration experiment with laser

Fig. 5a shows the energy distribution of the laser beam in a two-dimensional plane generated by the FM. By integrating the energy along Y-axis at each position on X-axis, an energy distribution along the X-axis is given (as later shown in Fig. 5d). Eq. (4) is the formula of this transformation:

$$Q(x) = \int q(x,y)dy \tag{4}$$

In this equation, $Q(x)$ is the one-dimensional energy distribution along X-axis, and $q(x,y)$ is the two-dimensional energy distribution on the plane.

Following the laser FM measurement, the same laser beam was measured using the SAC. Temperature data was collected by the SAC in the laser calibration experiment. After processing the temperature data using Eq. (1), histories of the energy that two anodes received were generated, as shown in Fig. 5b. The black coloured curve represents the received energy of the left anode, on which the plasma arc was started, whereas the red curve was the received energy of the right anode. Both curves present a stair-like shape because of the 30 s delay time of each increment. By calculating the averaged energy level difference between every two adjacent increments, as explained in Eq. (3), a laser energy distribution profile was constructed (Fig. 5c). We can see that, despite some slight fluctuations, the laser profile shows a bell-shaped energy distribution with a smooth curve. By comparing the multiple results from the repeated SAC measurement with the profile generated by the FM profiler in Fig. 5d, we can see that the shape of the SAC result matches the FM result very well with a similar root width of about 8 mm. A minor asymmetry caused by the slight divergence from the vertical position to the laser processing head is shown on the SAC profile. The overall energy density of the SAC profile is approximately 10% lower than that of the FM profile. This difference could be caused by two reasons. The first reason is that despite using heat-insulating material for the SAC device, a small amount of energy could be lost during the experiment. The second reason could be the reflection and radiation loss on the graphite coated surface. Nevertheless, the results of repeated SAC measurements show good consistency. Slight noise can be observed in these results. But it did not affect the overall shape of the energy distribution.

Two conclusions can be drawn from this laser calibration experiment. First, it demonstrated that the SAC has the capability of generating a clear and detailed profile of a stable laser and, therefore, can do the same for the profiling of a PTA if provided stably. The second is that the noise caused by the instrument is low and would not affect the measurement of an electric arc energy source.

3.2. Arc shape stability study

For PTA energy profiling, a PTA with a current of 130A was used, and the initial SAC setup was first tested. Both current and temperature data were collected during the process (Fig. 6a and b). Two energy distribution profiles of the arc were generated from these two dataset outputs. (Fig. 6c and d). Both the current and temperature data generated profiles show bell-like shape distributions. However, they are not very symmetrical, whereas an axial symmetric distribution would be expected, indicating that the arc shape was distorted during the measurement. The arc distortion was also confirmed by arc images. Fig. 7a and b are the images of the plasma arc before and after crossing the interface of the anode. It can be observed that the arc foot was stretched towards the interface. And the stretching direction gradually switched to the opposite direction when the arc crossed the interface. Repeated tests were conducted by reversing the moving direction of the torch, and the arc

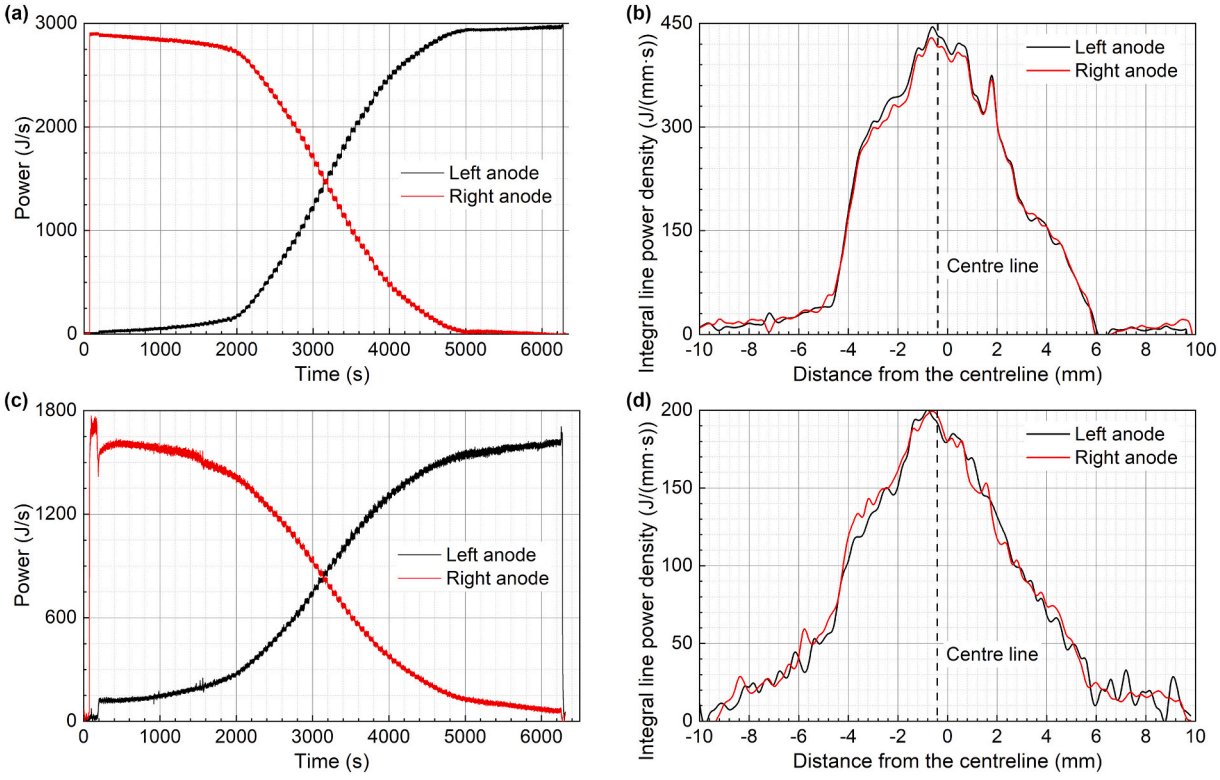

Fig. 6. Results of the initial SAC arc measurement: (a) energy that goes through two anodes calculated from the current data, (b) arc energy profile generated from the current data, (c) energy that goes through two anodes calculated from the temperature data, and (d) arc energy profile generated from the temperature data.

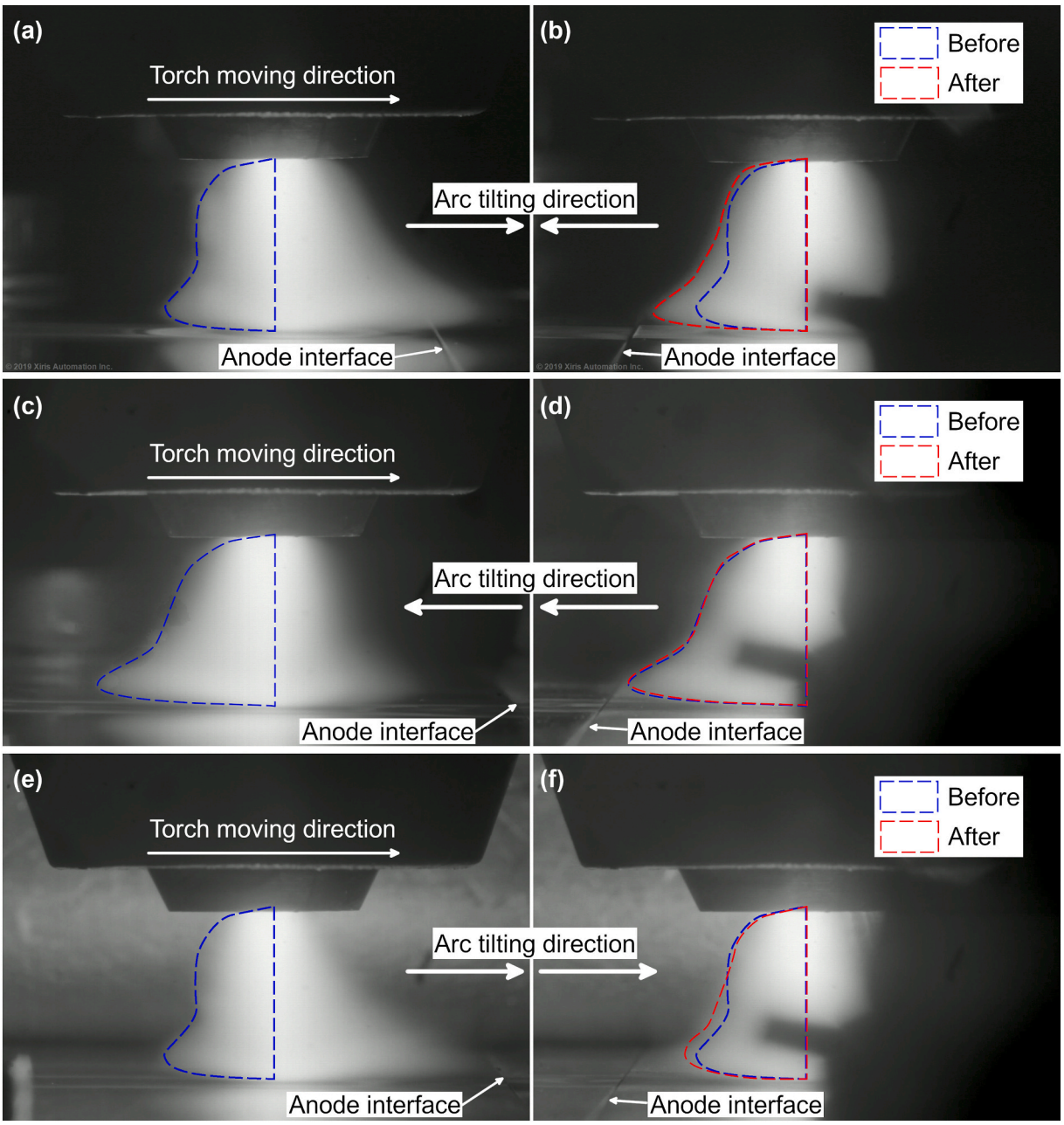

Fig. 7. Images of the arc before and after crossing the interface with different grounding conditions: (a) and (b) grounded at both sides with an insulated interface, (c) and (d) grounded at the right side with a connected interface, and (e) and (f) grounded at the left side with a connected interface.

foot was always stretched to the interface. There are three possible explanations for this effect. The first is that the plasma arc might be attracted to the edges of the copper anodes at the interface. It has been shown that arc root might lean to the edge of a substrate when approaching it due to a higher electron concentration at the sharp edge [25]. The second explanation is that electrical conductivity is zero at the interface, and the presence of this electrical barrier might influence the stability of the arc shape.

This kind of distortion seriously affects the quality of the measured profile. Different grounding conditions were tested to find out the cause of the arc stretching distortion. The arc images with a physically contacted interface and a single grounding were captured, either on the right anode (Fig. 7c and d) or the left anode (Fig. 7e and f). We can see that the arc shape was still slightly distorted. However, without the electrical barrier at the interface, the distorted shape stayed stationary during the traversing. In Fig. 7c and d, the arc foot stretched to the left when the grounding was on the right anode. In Fig. 7e and f, the arc foot was stretched towards the right when the grounding was on the left anode. Instead of being 'attracted' by the interface, the arc foot consistently pointed to the opposite side of which the grounding was located. It should be noted that removing the insulation between the anodes only slightly changed the gap distance of the interface. The fact that the dynamic shape changing disappeared completely when connecting the anodes proves that the shape of the interface has little to do with the arc distortion. Previous manuscripts mentioned that arc root would be blown to the opposite side by the electromagnetic field associated with the current flow when getting close to an asymmetric ground return connection [1,26]. Based on the correlation between the ground position and the arc stretching direction, it can be concluded that the arc stretching distortion was caused by off-centre grounding.

In the experiment using the modified SAC setup, the hypothesis that grounding position affects arc shape was further verified. Images of arc

were captured during the modified SAC measurement (Fig. 8c and d). It can be observed that slight distortion of the arc shape is still present when using the modified SAC. However, by comparing them to the arc images from the initial SAC (Fig. 8a and b, same as Fig. 7a and b), we can see that the overall arc shape distortion was significantly reduced. And the dynamic distortion of the arc shape upon crossing the interface was also mitigated.

Fig. 9 compares the current and temperature data generated profiles generated by the modified SAC and the initial SAC. The improvement in the arc stability was reflected in the energy profiles. Both the current and the temperature data generated profiles show more symmetric bell-like shape distributions compared to the previous profiles. The top of the modified SAC profile is rounder and evener, while the previous profiles were irregular at the top. The arc foot is also more symmetric. The width of the modified SAC current data generated profile is a bit more concentrated than the previous profiles without the distorted arc foot, indicating that the stretching distortion was reduced. The overall traversing was rather even and smooth with less lagging, and more accurate arc profiles were captured.

3.3. Repeated measurement of plasma arc

Repeated measurements of PTA with current of 130A were carried out with the improved system. In Fig. 10a and b, the results of nine measurements are shown. Data from each measurement are indicated as thin coloured lines, and the averaged results are shown as bold black curves. The outcome is still varying for each individual measurement. A few fluctuations appeared in some of the results. Some fluctuations appeared at the same positions on both the current data generated profile and the temperature data generated profile. Considering the results of the laser calibration experiment have significantly smaller fluctuation when measuring a stable laser beam, it is reasonable to conclude that these fluctuations are caused by the arc behaviour. The torch was directly driven by the linear actuator with a repeating accuracy of 63 μm to ensure that it was moved in even increments. A possible explanation for the fluctuation is that the arc root might not strictly follow the torch due to the limited stiffness of the plasma body. It is difficult to ensure that the arc root is moved in exact equal increments. A slight random defect seems to be unavoidable for each individual measurement. Nevertheless, the averaged profile shows a rather smooth and symmetric outline, indicating that the signal can be improved by averaging several measurements to overcome the random fluctuations. The averaged current density profile and the temperature distribution profile are compared in Fig. 10c. The temperature data generated profile peak energy level is about 47% of the current data generated profile peak energy level. The overall width of the temperature data generated profile is wider than the current data generated profile, whereas the current data generated profile has a more concentrated column. The column of the temperature data generated profile presents a more conical shape with a sharper top. The descending at two sides is slower with a wider out-reaching foot. Previous researchers have also found a similar phenomenon showing that the energy transferring area is generally more extensive than the current-conducting area [14,17]. This can be explained by the fact that although the current density is the dominating factor in the temperature distribution within an anode, other energy transfer mechanisms such as radiation and convection of hot gases also have a noticeable effect on heat transfer. Evans et al. [26] measured a 100 A PTA and demonstrated that 11% of the arc power was transmitted by the shielding gas, 16% was transferred by the plasma gas, 4.2% by electron thermal energy and 20% by anode effects, which added up to total energy efficiency of 51.2%. These mechanisms will reduce the temperature gradient between different zones and smoothen the temperature distribution. The total energy amount of the profile is calculated by integrating the area of the energy profile. By dividing the total

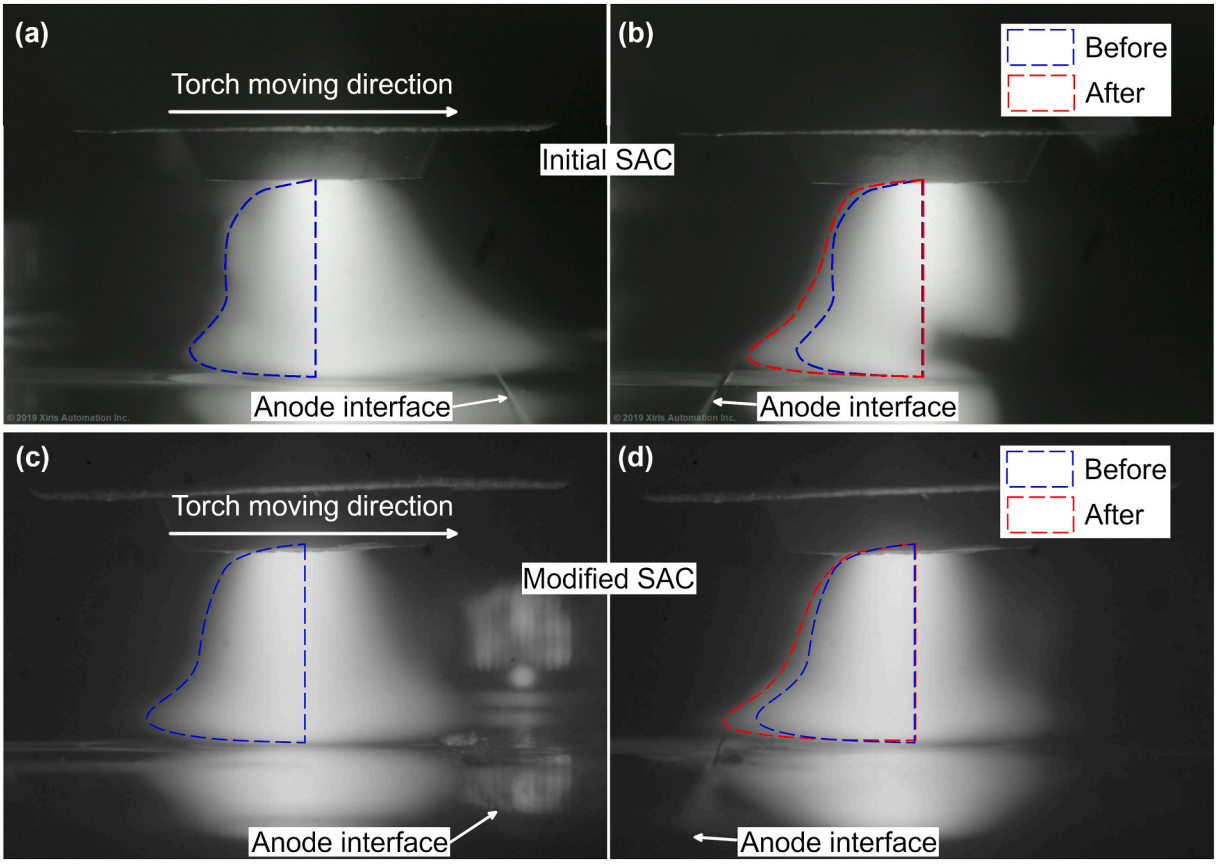

Fig. 8. Images of the arc before and after crossing the interface: (a) and (b) with the initial SAC, and (c) and (d) with the modified SAC.

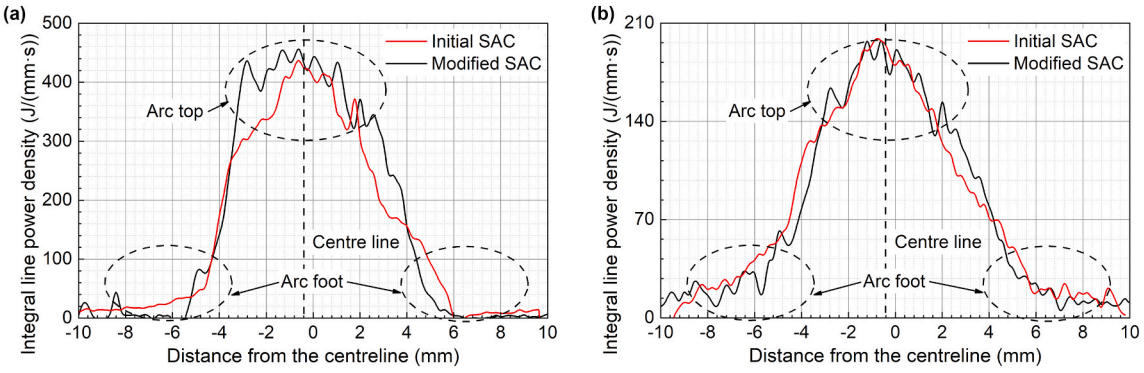

Fig. 9. Comparison of the profiles generated by initial and modified SAC: (a) current data generated profiles, and (b) temperature data generated profiles.

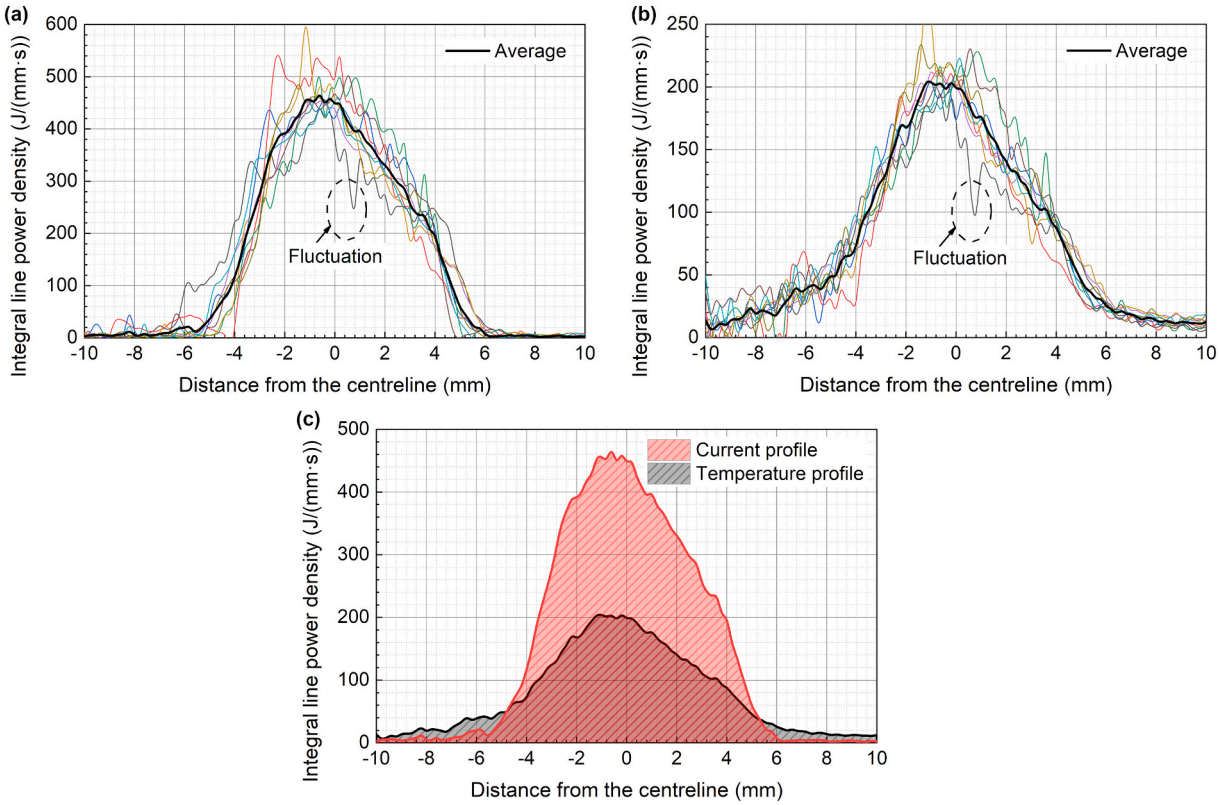

Fig. 10. (a) Repeated current measurements results, (b) repeated temperature measurements results, and (c) comparison between the current and temperature data generated profiles.

energy amount of the temperature data generated profile with that of the current data generated profile, an arc efficiency of 56% was obtained. This arc efficiency matches with the results in some previous literature on PTA measurement [13,26–28]. Some literature also reported higher PTA arc efficiency [29,30]. Inconsistent arc efficiency being reported might be due to different experimental parameters, such as current intensity, plasma gas flow rate, shielding gas flow rate, nozzle orifice size, etc. Another factor worth noting is that the energy profiles generated from the current data assumed that the voltages of the two anodes were the same. Nevertheless, previously in the laser calibrating experiment, we have shown that the temperature data generated profile reflects the actual laser energy density accurately. Based on this, we can infer that the temperature data generated profile directly reflects the energy delivered to the anode surface.

3.4. Comparison of the measured profile with Gaussian model

In Fig. 11a, Gaussian distributions with r of 5.5, 6.0, 6.5 and 7.0 and placed together with the current data generated profile. Among these different Gaussian profiles, we can see that the Gaussian profiles can eclectically match the measured current data generated profile with a similar range and shape when $r = 6.5$ with a higher PCC. However, the Gaussian distribution has a sharper and higher peak, while the SAC profile has a broader and rounder top and drops more steeply at both sides.

An efficiency factor η of 56% was implemented to the Gaussian profiles to meet the energy amount of the temperature data. Gaussian distributions with r of 6.5, 7.0, 7.5, and 8.0 are compared with the measured temperature data generated profile in Fig. 11b. The Gaussian profiles fitted the measured profile quite well. Particularly, PCC was higher when given an r of 7.0 mm but with a slightly higher peak value,

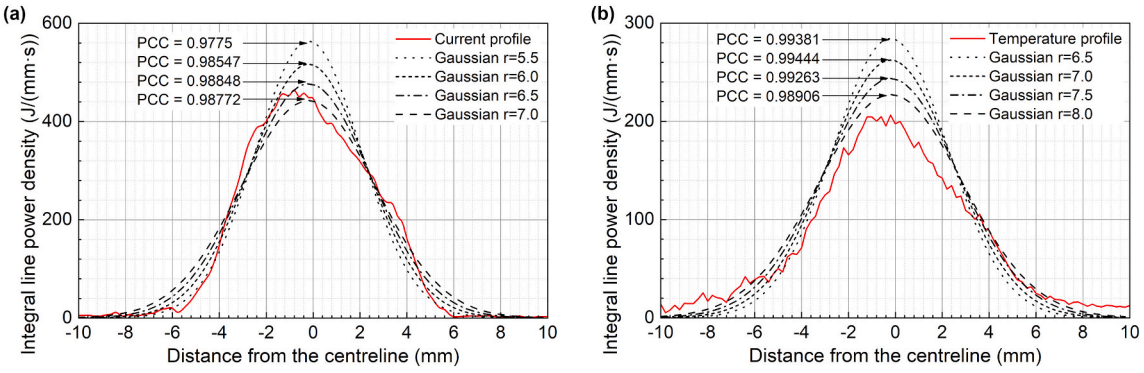

Fig. 11. Measured profiles fitted with Gaussian profiles: (a) current data generated profile and (b) temperature data generated profile.

while a larger r of 8.0 allows it to better match the peak value of the measured profile. The shape of the temperature data generated profile is more like the Gaussian profiles with similar top geometry and descending trend. However, with these results, we can confirm that the Gaussian model is usable with a plasma gas flow rate of 0.8 L/min and orifice size of 3.9 mm, which were used in the wire + arc additive manufacturing that requires a low arc pressure to avoid keyhole defects. However, it should be noted that the shape of the arc energy distribution may not always be similar to a Gaussian model. In welding and cutting applications, the plasma gas flow rate is usually higher and with a smaller orifice size to achieve higher penetration. Especially for thick plate welding, for example, plasma gas flow rate is about 2 to 10 L/min with an orifice size of about 3 mm [31]. So, the arc dimension demonstrated in the measured profile in this study is relatively broader and more like the dimension of a tungsten inert gas arc, as reported in the works of Nestor [13] and Schoeck [14].

4. Conclusions

From the investigations conducted and the results discussed above in this study, some conclusions can be summarised:

1. A laser beam measured by the hollow needle diagnosis system can be used to calibrate the SAC method. It showed that the SAC has the capability of generating a clear and detailed energy profile of a laser and, therefore, of a stable electric arc.
2. Ground wire position has a significant influence on the arc behaviour in the SAC. Centralised and even distances to the spatial arc section and the ground wire location reduce the arc distortion during the interface traverse, and a more symmetrical profile can be generated.
3. Slight fluctuations of the measured profile were not due to instrument noise but caused by erratic movement of the arc root. This kind of erratic movement is likely caused by incomplete rigidity of the plasma body and is therefore unavoidable. Still, defects of the individual profiles can be mitigated by averaging the repeated measurement results.
4. The plasma column of the current data generated profile is more concentrated and narrower than the temperature data generated profile. And the temperature data generated profile that was calibrated by the laser experiment is shown to reflect the energy absorption distribution of the arc directly. The absorption rate of the arc energy in this study is about 56%. A Gaussian model fits the measured profile well with a radius of about 7 mm.

Data Statement

Data underlying this study can be accessed through the Cranfield University repository at https://doi.org/10.17862/cranfield.rd.19555225.v1.

Declaration of competing interest

The authors declare the following financial interests/personal relationships which may be considered as potential competing interests: Guangyu Chen report financial support was provided by China Scholarship Council. Stewart Williams reports financial support was provided by Engineering and Physical Sciences Research Council.

Acknowledgement

Guangyu Chen would like to express his gratitude to Cranfield University, United Kingdom and China Scholarship Council, China (No. 201706680064) for funding his research studies. The authors would like to thank New Wire Additive Manufacturing (NEWAM), United Kingdom (EP/R027218/1) program for financial support. The authors also would like to thank Flemming Nielsen, Nisar Shah and John Thrower for the technical support.

References

[1] Weman K. Welding processes handbook. Second edition 2011. https://doi.org/10.1533/9780857095183.
[2] Thornton MF. Spectroscopic determination of temperature distributions for a TIG arc. J Phys D Appl Phys 1993;26. https://doi.org/10.1088/0022-3727/26/9/014.
[3] AJD Farmer, Haddad GN. Rayleigh scattering measurements in a free-burning argon arc. J Phys D Appl Phys 1988;21. https://doi.org/10.1088/0022-3727/21/3/008.
[4] Murphy AB, AJD Farmer. Temperature measurement in thermal plasmas by rayleigh scattering. J Phys D Appl Phys 1992;25. https://doi.org/10.1088/0022-3727/25/4/009.
[5] Haddad GN, AJD Farmer. Temperature determinations in a free-burning arc. I. Experimental techniques and results in argon. J Phys D Appl Phys 1984;17. https://doi.org/10.1088/0022-3727/17/6/015.
[6] Richardson IM. Properties of the constricted gas tungsten (plasma) welding arc at elevated pressures. Cranfield Institute of Technology, School of Industrial and Manufacturing Science; 1991.
[7] Olsen HN. The electric arc as a light source for quantitative spectroscopy. J Quant Spectrosc Radiat Transf 1963;3. https://doi.org/10.1016/0022-4073(63)90015-3.
[8] Cram LE, Poladian L, Roumeliotis G. Departures from equilibrium in a free-burning argon arc. J Phys D Appl Phys 1988;21. https://doi.org/10.1088/0022-3727/21/3/007.
[9] Gomes AM. Criteria for partial LTE in an argon thermal discharge at atmospheric pressure; validity of the spectroscopically measured electronic temperature. J Phys D Appl Phys 1983;16. https://doi.org/10.1088/0022-3727/16/3/019.
[10] Bober L, Tankin RS. Investigation of equilibrium in an argon plasma. J Quant Spectrosc Radiat Transf 1970;10. https://doi.org/10.1016/0022-4073(70)90119-6.
[11] Mott-Smith HM, Langmuir I. The theory of collectors in gaseous discharges. Phys Rev 1926;28. https://doi.org/10.1103/PhysRev.28.727.
[12] Fanara C, Richardson IM. A Langmuir multi-probe system for the characterisation of atmospheric pressure arc plasmas. J Phys D Appl Phys 2001;34. https://doi.org/10.1088/0022-3727/34/18/302.
[13] Nestor OH. Heat intensity and current density distributions at the anode of high current. Inert Gas Arcs. J Appl Phys 1962;33. https://doi.org/10.1063/1.1728803.
[14] Schoeck PA. An investigation of the anode energy balance of high intensity arcs in Argon. Mod. Dev. Heat Transf. 1963. https://doi.org/10.1016/b978-0-12-395635-4.50017-6.

[15] Egerland S, Colegrove P, Williams S. Investigation of low current gas tungsten arc welding using split anode calorimetry. Sci Technol Weld Join 2017;22. https://doi.org/10.1080/13621718.2016.1189214.
[16] Vilarinho LO, Fanara C. A modified split-anode detector for the study of the anode region of atmospheric pressure arc plasmas. Meas Sci Technol 2004;15. https://doi.org/10.1088/0957-0233/15/1/010.
[17] Tsai N. Heat distribution and weld bead geometry in arc welding. Massachusetts Institute of Technology; 1983.
[18] Suder WJ. Study of Fundamental Parameters in Hybrid Laser Welding. 2011.
[19] Beyer E, Herziger G, Kramer R, Loosen P. A diagnostic system for measurement of the focused beam diameter of high power CO2 lasers. 2018. https://doi.org/10.2351/1.5057866.
[20] Schwede H, Märten O, Kramer R, Wolf S, Brandl V, Hänsel K. Characterizing high-power laser beams to detect the thermal load of optics and to identify limitations within the design of the optical system. Solid State Lasers XVIII Technol. Devices 2009;7193. https://doi.org/10.1117/12.808951.
[21] Schwede H. Observe the beam at the center of interest. Laser Tech J 2010;7. https://doi.org/10.1002/latj.201090008.
[22] Kramer R, Schwede H, Brandl V, Wolf S, Märten O. Laser beam diagnostics according to ISO and their impact on practical application. Opt. Des. Eng. II 2005;5962. https://doi.org/10.1117/12.639286.
[23] ISO11146-1. ISO1146-1 Test methods for laser beam widths, divergence angles and beam propagation ratios. Int Stand 2005;1.
[24] Pearson K. Mathematical contributions to the theory of evolution. Proc R Soc 1896;60.
[25] Lancaster JF. The physics of welding. Phys Technol 1984;15. https://doi.org/10.1088/0305-4624/15/2/I05.
[26] Evans DM, Huang D, McClure JC, Nunes AC. Arc efficiency of plasma arc welding. Weld J (Miami, Fla) 1998;77.
[27] JN DuPont, Marder AR. Thermal efficiency of arc welding processes. Weld J (Miami, Fla) 1995;74.
[28] Fuerschbach PW, Knorovsky GA. A study of melting efficiency in plasma-arc and gas tungsten arc-welding. Weld J 1991;70.
[29] Haelsig A, Kusch M, Mayer P. New findings on the efficiency of gas shielded arc welding. Weld World 2012;56. https://doi.org/10.1007/BF03321400.
[30] BS 1011-1-2009. BS 1011-1-2009 welding—recommendations for welding of metallic materials—part 1: general guidance for arc welding. Bs En 1011-420003;2000.
[31] Norrish J. Advanced welding processes. 2006. https://doi.org/10.1533/9781845691707.

2022-04-16

Split anode calorimetry for plasma arc energy density measurement with laser calibration

Chen, Guangyu

Elsevier

Chen G, Williams S, Ding J, et al., (2022) Split anode calorimetry for plasma arc energy density measurement with laser calibration, Journal of Manufacturing Processes, Volume 78, June 2022, pp. 71-81

https://doi.org/10.1016/j.jmapro.2022.04.003